Fast Wafer-Level Characterization of Silicon Photodetectors by Photoluminescence Imaging

Hussein M. Ayedh, Christopher W. Förbom, Juha Heinonen, Ismo T. S. Rauha, Marko Yli-Koski, Ville Vähänissi, and Hele Savin

***Abstract*— Photoluminescence imaging (PLI) technique is conventionally used in silicon (Si) photovoltaics (PV) for device characterization and inline quality control, providing substantial assistance for a wafer-level process monitoring from as-cut wafers to fully fabricated devices. Surprisingly, employing this method has not spread outside PV, and thus, its potential remains largely unknown in other fields. In this case study, a fully processed Si photodetector wafer, consisting of photodiodes with various sizes, has been chosen as an example to explore the potential of PLI beyond PV. First, we show that the standard PLI measurement is able to provide a high-resolution full-wafer luminescence image of the complete devices only within a couple of seconds. The image reveals various types of inhomogeneities present in the devices, such as furnace contamination and other processing-induced defects. The measured data are then converted to an effective lifetime image followed by benchmarking with a conventionally measured recombination lifetime map obtained by microwave-detected photoconductance decay (μ-PCD), demonstrating further superiority of PLI in terms of the spatial resolution and the measurement time. Finally, correlation with diode leakage current and photoresponse measurements show that PLI is able to provide useful information on the final device performance without a need for traditional electrical contact measurements. While this study has focused on Si photodetectors, the results imply that PLI also has potential in other semiconductor devices for fast wafer-level process monitoring purposes as well as for a single device characterization either before or after wafer dicing.**

***Index Terms*— Photodetectors, photoluminescence imaging (PLI), process monitoring, recombination/generation lifetime, silicon (Si).**

I. Introduction

PROCESS monitoring and final device characterization play an important role in the semiconductor industry in both production and research and development. For silicon (Si) devices that require high purity, such as integrated circuits and photodiodes, the quality characterization of the starting material and the cleanliness of the fabrication processes are of utmost importance. Commonly used methods for such characterization include microwave-detected photoconductance decay (μ-PCD) [1] and surface photovoltage (SPV) [2], [3] as they offer contactless means to measure the carrier recombination and the diffusion length in the form of a recombination lifetime map. Despite their many benefits and wide utilization in the industry, these methods have a limited spatial resolution and throughput, which often limits their use to separate monitor wafers instead of characterizing actual device wafers at different stages of the process. Most importantly, the poor resolution of these techniques hinders their use in performance assessment of the final devices. This may lead to the situation that the root cause of device failure remains unknown.

It would be highly attractive to find a single method that is applicable to both final device characterization as well as process monitoring throughout the device fabrication. It is rather surprising that such a characterization requirement has been addressed in photovoltaics (PV), where diverse characterization methods have lately emerged even though the purity requirements are less stringent than in microelectronics. A good example is photoluminescence imaging (PLI) that was first introduced in 2005 by Trupke and Bardos [4]. This method has shown high robustness with reliable and repeatable results in revealing contamination and defects in the wafers [5]–[8] and consequently has become a key asset in the entire PV manufacturing chain as well as in research and development. The main benefit of this method is the capability of nondestructive and contactless measurements at various processing steps, including as-cut wafers and half-processed samples extending all the way to fully fabricated solar cells. This is accompanied by a high spatial resolution (typically $\sim$165 μm/pixel) and a short acquisition time of only a few seconds for capturing a full 6–8-in wafer [7]. These properties have enabled the identification of the source(s) of defects and their evolution during Si solar cell fabrication as well as quality sorting of the final cells [8]. All these characteristics would be highly beneficial also in the manufacturing of other semiconductor devices, and hence, the potential of the method beyond PV is worth investigating. Indeed, Duru *et al.* [9] have already started this by focusing on submicrometer-scale buried defects.

In this work, we study the applicability of PLI for the characterization of electronic devices that have high-purity requirements. As a case example, we take a Si photodiode

Manuscript received December 6, 2021; revised February 2, 2022; accepted March 8, 2022. Date of publication March 28, 2022; date of current version April 22, 2022. This work was supported in part by the Academy of Finland under Project 13331313 and Project 328482, and in part by the EMPIR program co-financed by the Participating States and from the European Union's Horizon 2020 Research and Innovation Program under Project 19ENG05 NanoWires. The review of this article was arranged by Editor R. Kuroda. *(Corresponding author: Hussein M. Ayedh.)*

Hussein M. Ayedh, Christopher W. Förbom, Ismo T. S. Rauha, Marko Yli-Koski, Ville Vähänissi, and Hele Savin are with the Department of Electronics and Nanoengineering, Aalto University, FI-02150 Espoo, Finland (e-mail: hussein.ayedh@aalto.fi).

Juha Heinonen is with ElFys Oy, FI-02150 Espoo, Finland.

Color versions of one or more figures in this article are available at https://doi.org/10.1109/TED.2022.3159497.

Digital Object Identifier 10.1109/TED.2022.3159497

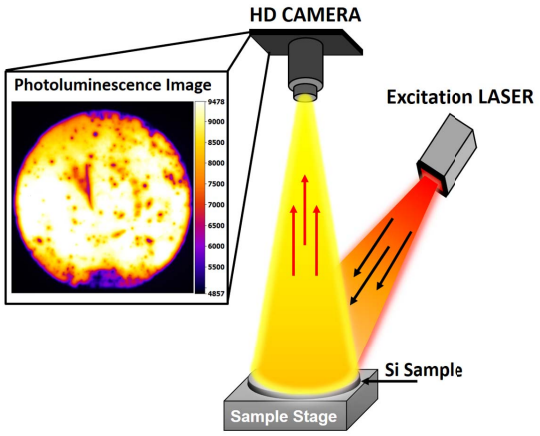

Fig. 1. Schematic illustrating the basic concept of PLI and the main components involved in the measurement system. The inset shows an example of an acquired PL image of a bare silicon wafer showing multiple dot-like defects.

wafer processed in a standard cleanroom environment. We start by introducing the theory of PLI, including its operation principle. Then, we study the potential of the method in revealing possible inhomogeneities and defects within the wafer as well as in the individual detector chips. We compare the results to more conventional characterization methods, such as μ-PCD, dark/leakage current density (J_{dark}), and photoresponse [external quantum efficiency (EQE)] measurements. Finally, based on the obtained results, we discuss the benefits and limitations of PLI when using it beyond PV.

II. Methods and Experimental Details

A. Background

The basic operation principle of PLI is based on the well-known photoluminescence phenomenon (see Fig. 1), where charge carriers are excited in a semiconductor material with an external light source and the resulting luminescence (light emission), due to subsequent recombination of carriers, is captured by a high-sensitivity camera. In more detail, the measurement begins with excitation by light, whose intensity, or rather the corresponding absorption in the sample, determines the photogeneration rate (G_{ph}). The photogeneration is balanced with the carrier recombination leading to a specific quasi-steady-state excess carrier density (Δn). As is well known, the recombination takes place via different mechanisms, such as trap-assisted [Shockley–Read–Hall (SRH)], Auger, surface, and band-to-band recombination [10]–[15], which together determine the sample-specific effective recombination lifetime (τ_{eff}) [16]. Out of all these recombination mechanisms, only direct band-to-band recombination is detected by the camera. (Please note that it is also possible to measure defect-to-band PL [9], but here, we focus only on band-to-band PL.)

In Si, due to the indirect bandgap, the radiative recombination is very weak and highly dependent on the other mechanisms as shown in the following equation [17], [18]:

$$U_{\text{rad}} = B\left(n \cdot p - n_i^2\right) \tag{1}$$

where U_{rad} is the rate of radiative recombination, B is the radiative recombination coefficient, n and p are the electron and hole concentrations, respectively, and n_i is the intrinsic carrier concentration. For instance, if the SRH recombination dominates (n and/or p are reduced), the radiative recombination and the corresponding luminescence signal diminish. Consequently, the PL image correlates with τ_{eff}, and a low PL count per pixel (dark pixel) in the acquired image indicates a high total recombination rate i.e., a low effective lifetime, and vice versa. Thus, as an output, the method gives an image, from which one can easily see the defects that are recombination active. They can be present either in the bulk, junction, or at the surfaces of the wafer. For clarity, hereinafter, the phrases recombination and lifetime refer to the total recombination and total recombination lifetime, which have a direct correlation to the material quality.

The measurement of the PL signal brings both benefits and drawbacks compared to the traditional methods that rely on the measurement of the sample photoconductance. In addition to the fast measurement and high spatial resolution, a substantial benefit of measuring luminescence is related to low injection conditions: the method is insensitive to trapping of minority carriers and the so-called depletion region modulation, which are known to be common artifacts present often in the traditional photoconductance [19]–[21]. The main drawback is that although the measured photoluminescence signal (I_{pl}) correlates with the lifetime, absolute lifetime values cannot be directly obtained. This is because

$$I_{\text{pl}} = k \cdot U_{\text{rad}} = k \cdot B\left(n \cdot p - n_i^2\right) \tag{2}$$

where k is a scaling factor. At low injection, this reduces to $I_{\text{pl}} = k_1 \cdot \Delta n \cdot N_{D/A}$, and at high injection, this reduces to $I_{\text{pl}} = k_1 \cdot \Delta n^2$, where k_1 is a constant and $N_{D/A}$ is the doping concentration [22], [4]. However, since $\Delta n = G_{\text{ph}} \cdot \tau_{\text{eff}}$, it is rather straightforward to find the calibration coefficient k_1 by performing a separate carrier lifetime measurement in a single location of the sample, e.g., by a photoconductance method [1], [23], [24]. The details of the calibration procedure are explained, e.g., in [25] and [26]. After this calibration, the PL image can be directly converted into a lifetime image. Note that the fact that I_{pl} depends on G_{ph} may raise the need for a further calibration, e.g., in the case of varying excitation intensity and/or the optical properties of the sample.

Until now, PLI has been mainly used in PV where the devices (Si solar cells) have uniform optical properties. This results in a laterally uniform photogeneration rate over the whole wafer area, which makes the calibration process relatively simple. Furthermore, the impact of the recombination lifetime on the final device performance is rather straightforward as solar cells operate at a positive bias voltage resulting in a narrow depletion region. Consequently, the charge collection takes place mostly via diffusion from the bulk, where the carrier recombination plays a critical role leading to a direct correlation with the solar cell performance. Characterization of devices that operate at reverse bias voltages and/or require a high speed, including photodetectors, deviates from that of solar cells to some extent; While in solar cells, diffusion current plays an important role, in detectors, the signal

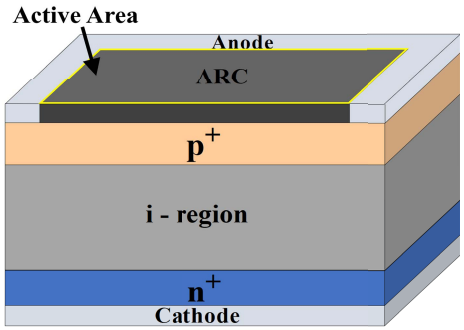

Fig. 2. Cross section of the studied Si p-i-n photodiodes (photodetectors).

collection is dominated by the charge-carrier drift induced by the electric field. Despite this difference, it is well known that the recombination losses in the depletion region as well as at the surfaces impact directly the photocurrent of the detectors similarly as in the solar cells. Consequently, the PL image should give valuable information about the response of the device in each point of the wafer.

Another interesting difference is that the purity requirement and tolerance to the defects both in the bulk and at the surface of the wafer are more stringent for the photodiodes than for the solar cells. This is because in reverse biased detectors, the so-called dark current, i.e., the noise signal, is affected by thermal generation inside the depletion region and carrier diffusion from the quasi-neutral regions. Both of these are affected by imperfections such as interface and crystal defects, metal contamination, implantation damage, trench isolations, etc., and more precisely their generation and recombination properties determined by capture cross sections and position in the bandgap [27], [16]. Since PL measures recombination under optical excitation, the measurement does not necessarily correlate with the dark current. This is because not all the recombination centers act as effective generation centers [16]. Therefore, it will be interesting to see how well PLI is able to reveal the defects contributing to the dark current.

B. Samples and Measurements

In this work, we use Si p-i-n photodiodes (photodetectors) as a case example of high-purity devices to be characterized by PLI. Fig. 2 shows a typical cross-sectional view of a single Si photodetector. The active area on the front side has often antireflective coating (ARC) typically optimized for a specific wavelength accompanied with a surface passivation layer to reduce the surface recombination. The active area is surrounded by a narrow metal contact ring (anode), and the rear surface of the wafer is fully covered with a metal layer that forms the cathode of the device. In photodiodes, the charge-carrier separation is realized with a p-n junction similar to a solar cell. The substrate is often a high-resistivity wafer that enables a higher lifetime and a wider depletion region under reverse bias. The wafer selected for this study contains p-i-n photodiodes with four different sizes manufactured on a 6-inch Si wafer having areas of 100, 25, 4, and 1 mm^2.

For the PLI measurement, a commercial BT imaging LIS-R2-plus PL imaging system designed for Si solar cell characterization was employed. The used PLI system is equipped with a monochromatic excitation laser of 915 nm wavelength with the beam spread over the 165 mm $\times$ 165 mm area on the measurement stage for homogeneous illumination. The used excitation photon flux was varied between 0.25 - 1 $\times$ 10^{18} $cm^{-2} \cdot s^{-1}$. The photoluminescence signal was captured with a high-definition Si charge-coupled device (CCD) camera with two sets of imaging lenses: a standard lens leading to a resolution of $\sim$165 μm/pixel for capturing images of the entire wafer (the field of view is 165 $\times$ 165 mm^2) and a high-magnification lens leading to a resolution of $\sim$30 μm/pixel for a particular focus on a small area (the field of view is 30 $\times$ 30 mm^2). In order to present the data as a recombination lifetime image (focus on quantitative values in the active areas), the corresponding calibration coefficient was determined by measuring the recombination lifetime in the middle of a single chip using a 1 mm^2 μ-PCD spot.

The obtained lifetime images were compared with results from conventional characterization methods for overall benchmarking purposes but also for the observation of a possible overlap and/or complementary characteristics. First, we characterized the photodetector wafer with μ-PCD mapping that is commonly used in the integrated circuit and the wafer manufacturing industry for monitoring the quality of the starting material and the process cleanliness. A full-wafer μ-PCD lifetime scan was performed with a raster size of 0.5 mm, an averaging of 16 measured values, and the microwave transient signal with a frequency of 10.367 GHz. The lifetime map obtained with μ-PCD was then compared to the lifetime image obtained by PLI to see the differences between the methods. Second, we characterized the photodetectors with the common electrical detector characterization methods, namely, the dark current and EQE measurements. The former was performed using an automated probe station by applying voltages from -20 to 2 V in steps of 0.5 V and by recording the current–voltage (I–V) curves in the dark. A special focus was placed on the determination of the dark current at -5 V. The EQE measurements were performed to see the correlation of the photoresponse to the PLI at specific wavelengths. For these measurements, selected photodetectors were diced from the wafer and glued on a standard printed circuit board. The EQE measurements were made using a halogen lamp coupled to a monochromator for selecting the desired wavelength to be focused on the photodetector surface. The output current of the illuminated photodetector under 0 V bias was recorded and the EQE was obtained by comparing the current values to a calibrated reference photodetector.

III. Results and Discussion

A. Qualitative Characterization

Fig. 3(a) shows a photograph of the studied wafer. The active areas of the photodetectors are clearly distinguishable by the naked eye as black squares (due to the low reflection surface) and their different sizes become apparent as well. The surrounding areas have planar silicon surface showing a much

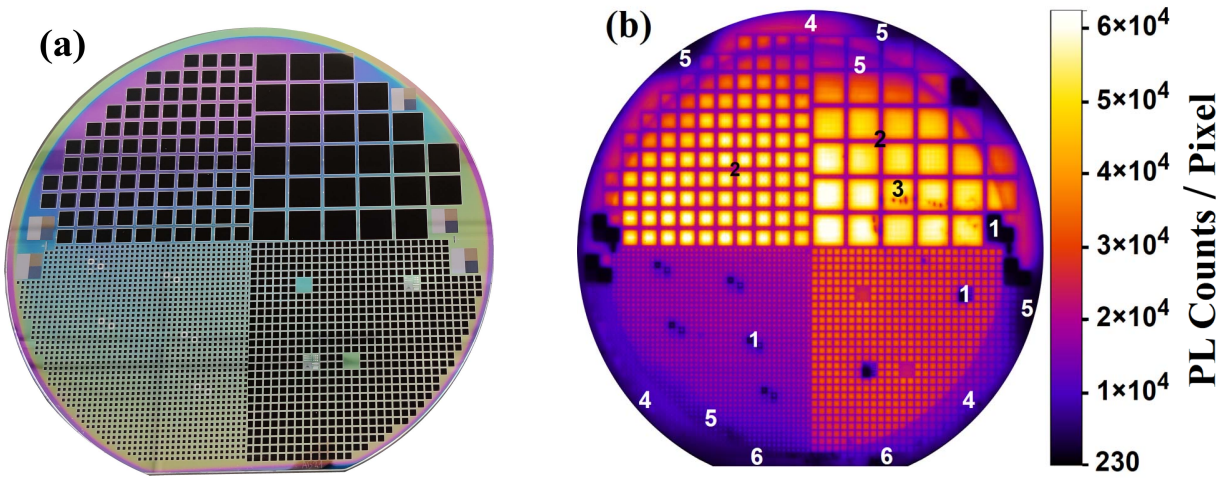

Fig. 3. (a) Photograph of the 6-inch Si wafer having four different photodetector sizes, each in its own quarter. Black areas represent the device active areas. Some reflections from the ceiling are visible on the planar areas and/or the metallized parts of the wafer. (b) PL image of the same wafer. Bright areas correspond to high PL counts per pixel and dark areas represent low PL counts per pixel as shown in the scale bar. Individual dark chips consist of test structures with metallic layers on top. The marked numbers refer to different defects that are discussed in the text.

higher reflectance. Additional test structures are also visible on the wafer surface (small mirror-like squares with a metallized surface). Fig. 3(b) shows the same wafer imaged by the PLI technique, employing a standard lens. The photodetector chips and the test structures are clearly distinguishable also in the PL image. The dark areas associated with the test structures appear black as they have metal layers on top, which blocks the excitation light (marked as #1), while the dark lines between the chips (#2) are due to a lower photogeneration rate in the planar than in the black surface (due to a difference in the absorption of the excitation light). Consequently, the active areas stand out similarly as in the photograph, making the identification of specific chips straightforward.

As expected, the active areas show, in general, rather high and uniform PL signal since these areas are designed to convert the incident photons into electron-hole pairs, and any recombination there would likely affect the device performance. However, upon a closer inspection, it is clear that many of the chips are not perfect. For instance, there are several different recombination active areas visible in the PL image: 1) the small dark spots in specific photodetectors at the upper right quarter (marked as #3); 2) the dark circle shown all around the wafer (#4); 3) the completely dark areas at the outermost edge of the upper half and the bottom right edge (#5); and 4) the dark areas with various sizes and shapes all around the wafer (#6). None of these defects are visible in the photograph of the wafer, so they are most likely resulting from the fabrication steps. In this study, the device wafer is measured only in its final form and, therefore, it is difficult to speculate the origin of these defects. However, the shape, size, and position of the dark areas may also reveal the source of defects. For instance, in this specific wafer, some circular wafer stages and the furnace boat contamination are likely the origins for the increased recombination in positions #4 and #5, respectively. In order to be sure about the origin of other defects, one should employ PLI as a process monitoring method between the process steps to pinpoint at what stage of the fabrication they were induced. Such identification of defects has already been demonstrated in the fabrication of crystalline Si solar cells [28], [29].

The above analysis was based on an image taken by the standard lens that enables capturing the luminescence from the entire wafer. To observe more details within individual chips, we made another image as shown in Fig. 4 by employing a high-magnification lens that focuses on a small area of the wafer. The image shows a clearly higher resolution with sharp features and displays an obvious quality variation within the chips that could not be observed with the resolution provided by the standard lens. It is also interesting to note that the Al bonding pads (dark dots) with a size of 150 × 300 μm^2 located at the left side of each chip edge become visible in this image. From a final application-centered point of view, the high-magnification PLI could be employed for a deeper inspection of the possible reasons behind the poor performance of selected chips. However, one needs to remember that like in all recombination-related measurements, if the diffusion length of the charge carriers is long enough, the lateral resolution is not limited by the measurement system resolution but by the diffusion length itself. Higher illumination intensity can be used to reduce this effect to some extent, but it will also reduce the overall recombination lifetime due to unavoidable Auger recombination. In this case example, the smaller PL counts close to the edges of the active areas seen in Fig. 4 are most likely due to carrier diffusion outside of the active area—not due to the recombination inside it.

B. Lifetime Image

While a qualitative characterization by PLI can be informative enough, sometimes, it is beneficial to present the measured PL data as a lifetime image to enable a more quantitative analysis. Furthermore, in our test wafer, one needs to pay

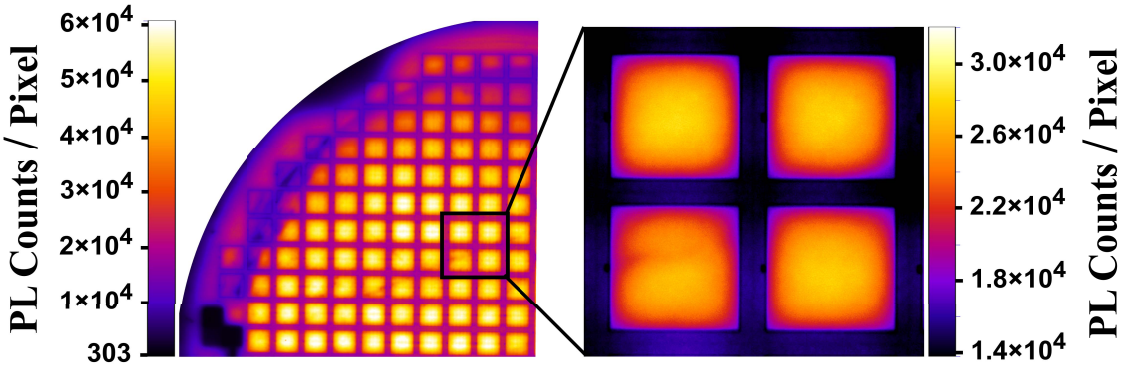

Fig. 4. PL image (left) captured by the standard lens for the upper left quarter of the studied wafer. The active area of a single detector chip is 5×5 mm^2 in this quarter. A high-magnification PL image (right) of a small specific area with 2×2 chips from the same quarter for comparison. Since both images are taken with the same camera, the number of pixels in each image stays the same resulting in significantly increased spatial resolution.

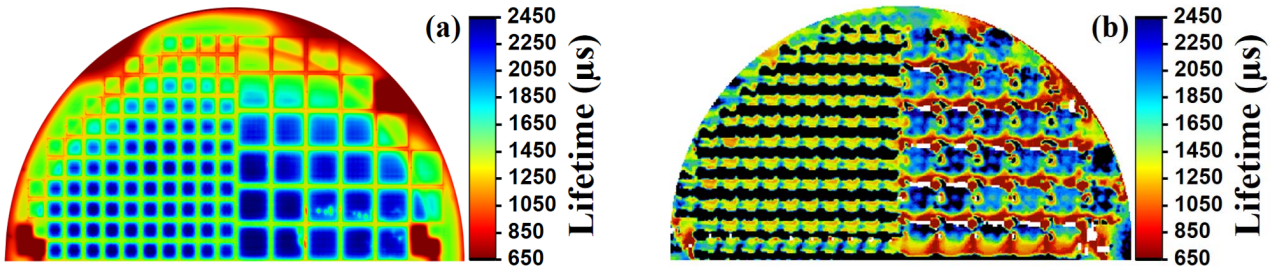

Fig. 5. Lifetime image of the upper half of the studied wafer measured with (a) PLI with an acquisition time of 3.5 s and (b) μ-PCD scanning with a measurement time exceeding 6 h.

special attention to the different photogeneration rate outside and inside the active areas. Fig. 5(a) shows a lifetime image of the upper half of the same photodetector wafer measured by PLI. It can be seen that the effective lifetime is about 2.5 ms at the active area in the majority of the devices, whereas the outermost diodes have significantly lower lifetimes (<1.5 ms). The small, localized recombination defects in the right quarter show a lifetime value of about 1.6 ms. When looking at the contamination from the oxidation furnace (previously marked as #5), we can see that the lifetime is significantly lower than elsewhere, but as mentioned above, a quantitative lifetime value here should be interpreted with care as this edge area has a different photogeneration rate due to the different surface reflectance. Nevertheless, all these values should provide useful benchmarking information for the detector manufacturers as they could define a certain threshold value for the lifetime depending on the requirements for the final application. As an example, in some applications, chips with an effective lifetime below 1.5 ms might not be acceptable.

For reference purposes, Fig. 5(b) presents the recombination lifetime map of the same wafer measured by a μ-PCD scanner. We can immediately see the similarities and the differences between the measurements. First, μ-PCD has severe limitations in measuring the small chips, and in fact, the lower half of the wafer could not be measured at all. Even the second largest chips in the wafer (25 mm^2, the upper left quarter) could not be measured well as the metal contacts (dark blue rows) introduced serious artifacts to the measurements. Indeed, only the largest chips (100 mm^2, upper right quarter) manifested well the active areas of the photodetectors even though the spatial resolution is still highly limited, raising potential for false interpretation. As an example, the μ-PCD lifetime map at the bottom and top rows shows a lifetime behavior that is completely opposite to that seen in the PL lifetime image. Since it is well known that typically, the outer edges of the wafers suffer from higher recombination, the PL lifetime data are probably more reliable. While the main advantage of μ-PCD is that the measurement does not need a separate calibration, its measurement time is very slow: a PL image takes only 4 s or even less for acquiring the image of a full wafer, whereas a μ-PCD map needs several hours for scanning the whole wafer.

The above results demonstrate that PLI is an efficient method to characterize the effective lifetime of fully processed detector chips - even in the case of a relatively small chip size. Regarding a qualitative PL count image versus a lifetime image, qualitative PL data are likely enough for most detector manufacturers, e.g., for a batch-to-batch comparison (assuming that the photogeneration rate is kept constant). However, quantitative lifetime values and the corresponding image may turn out useful, especially when a specific threshold level for the lifetime can be appointed or when the optical properties vary a lot within or between the wafers.

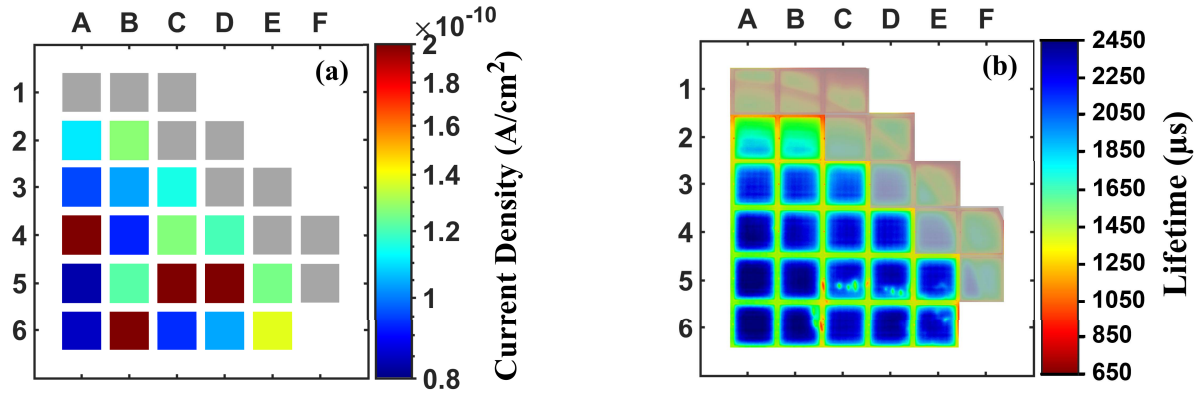

Fig. 6. (a) Leakage current measurements on the upper right quarter of the studied wafer. The gray chips were not measured. (b) Lifetime image of the same chips obtained by PLI.

C. Comparison to the Dark Current

One of the most important device parameters in the photodiode industry is the dark current density (J_{dark}) under a reverse bias voltage as it describes the noise level of the final device. J_{dark} is expected to be dominated by both generation and recombination centers, and therefore, a direct correlation with the PLI is not expected but is worth investigating.

The I–V measurements showed typical diode characteristics in most of the photodetectors with J_{dark} in the range of 10^{-10} A/cm^2 measured at -20 V. However, there were several chips that suffered from a much higher J_{dark} ($\sim 10^{-8}$ A/cm^2). For simplicity, we plot in Fig. 6(a) J_{dark} measured at -5 V from the photodetectors located at the upper right quarter of the test wafer. As can be seen, in this quarter, four photodetectors suffered from high leakage (red chips), while the majority of the photodetectors had a very low J_{dark} at this voltage. A few chips close to the edges had J_{dark} somewhere in between.

The lifetime image taken by PLI for the same chips is shown in Fig. 6(b) allowing for an easy comparison between the methods. Interestingly, a correlation between these two measurements can be observed. The photodetectors close to the center of the wafer have generally higher lifetime (>2.5 ms) and lower J_{dark} (blue chips), while the ones closer to the edge of the wafer turn slightly worse in both measurements (light blue/green, lifetime $<$ 1.5 ms). The very outermost chips near the edges were skipped by the I–V measurements due to a lower quality indicating a good correlation with the PL image since, in these areas, the lifetime is even below 1 ms. It is also interesting to note that the chips with the highest J_{dark} (dark red; B6, C5, and D5) correspond to the chips that contain the spot-like defects in the active area clearly visible in the PL image (lifetime $\sim$1.5 ms). The only exception is the chip A4, which shows a homogeneous and high lifetime above 2 ms in the PLI measurement, while simultaneously being among the chips that show a high J_{dark}. The reason for this discrepancy could be, for instance, the leakage resulting from outside of the active area and, indeed, there is a small spot visible near the right edge of this chip. A high-resolution PL image could have been used to confirm this hypothesis.

It was surprising to see a relatively good correlation between J_{dark} and the PLI lifetime data, even though the former is measured in the dark at a reverse bias (depletion mode) where both the generation and recombination defects contribute, while the latter is measured under illumination where only the recombination prevails. On the other hand, it is well known that the energy level of the defect in the bandgap as well as the capture cross section determine whether the defect is a generation or recombination center - or both. In particular, the defects that are located near the mid-bandgap and whose capture cross-sectional properties for both carriers are symmetrical [16], [27] are known to cause both recombination and generation. If J_{dark} is limited by such defects, a strong correlation with the PLI is expected. Nevertheless, since there was no one-to-one correlation between the measured parameters, the I–V measurements cannot be fully replaced by the PLI in the future. However, the PLI may be able to reveal the reason for the high leakage due to a high spatial resolution that is not possible with bare I–V measurements.

D. Comparison to the EQE Measurements

In addition to J_{dark}, the actual signal, i.e., the photocurrent that is determined by the EQE, is often an important parameter in characterizing the performance of the photodetectors. Here, the PLI is expected to have a higher correlation with the EQE measurements than with J_{dark}, as both quantities are measured under illumination. In order to facilitate an easy comparison to the PLI, a single wavelength (550 nm) was selected from the EQE measurements, which corresponds to an absorption depth of $\sim$1.5 μm. Based on the PL image, four photodetectors were selected for the EQE measurements. The selected chips show different recombination characteristics as follows: 1) a high lifetime (A5); 2) a low lifetime (B2); and 3) localized defected areas with a low lifetime (C5). In addition, the contradictory chip (A4) that showed a high lifetime combined with high J_{dark} was selected as well. The EQE results of these chips are shown in Fig. 7. The dark current and the lifetime maps of the upper right quarter chips are shown in the same figure as insets.

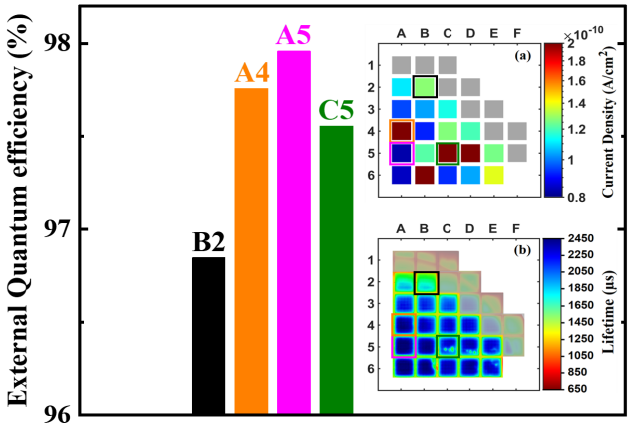

Fig. 7. EQE measured at 550 nm for selected chips from the upper right quarter of the studied wafer. The insets include the dark current map and PL lifetime image highlighting the selected chips.

Fig. 7 shows that the chip with a uniformly high lifetime (A5) corresponds to the highest EQE, while the low lifetime chip (B2) shows the poorest photoresponse. The photodetector with the spot-like defects (C5) shows a photoresponse in between. It is also interesting to notice that the contradictory chip (A4) that showed a high lifetime but had also a high J_{dark} shows a high photoresponse as well. This behavior indicates that this chip is affected by generation defects that control J_{dark} but not recombination defects. Alternatively, the defects contributing to the dark current are located outside the diode active area. Overall, it can be concluded that the PLI correlates well with the EQE measurements and, thus, the PLI could possibly even replace the EQE measurements if the exact photocurrent value is not needed.

Based on the above results (both the EQE and J_{dark}), it seems that the PLI could provide a fast means of screening the overall quality of the devices and preceding fabrication steps. Since the chips are typically tested individually after the fabrication, a fast qualitative characterization may save plenty of time, effort, and resources as the defective chips could be discarded already at an earlier stage without a need for characterization of the bad chips. The PL image could also be used to estimate the maximum yield per wafer. Furthermore, the PL image could reveal the source of the quality degradation for specific chips, which may not be possible with the conventional electrical measurements due to the absence of a high spatial resolution.

IV. Conclusion

In this contribution, we have studied whether the PLI method, which is widely used in research and development and in the manufacturing of Si solar cells, could be exploited more broadly for the characterization of other Si devices as well and, more specifically, what the possible benefits and challenges could be. Here, we took as an example a fully processed Si device wafer that consisted of hundreds of small photodiodes with varying sizes.

The first conclusion is that the PLI can, indeed, reveal interesting features on both wafer and chip level as various types of process-induced defects were revealed by the method. Furthermore, it turned out that the PLI allows much faster data acquisition and a higher spatial resolution compared to the other state-of-the-art methods. However, the interpretation of the raw data is more complicated than in the case of solar cells. The main challenge comes from the fact that there are often a lot of spatial variations within a wafer as it may have different surface coatings and thicknesses, which means that the photogeneration rate is not necessarily laterally uniform like that in the solar cells. This difference should be considered in the interpretation of the results. Nevertheless, with a known photogeneration rate or in the case of a homogeneous device area, the method is easy to use as even raw PL data may be able to reveal the source of the defects. Some manufacturers may find an additional lifetime calibration a useful option to define a threshold value for a specific process step (or at the end of the device fabrication) allowing for a fast quality sorting of the processed microchips. Overall, a batch-to-batch comparison should be relatively straightforward even without the need for a separate lifetime calibration.

In the case of photodetectors, we showed that the PLI cannot fully replace the electrical leakage current measurements, at least not without a deeper inspection, as the leakage current may also originate outside the active area, where the defects can be more difficult to observe by the standard lens. One also has to pay special attention to whether the signal collection (EQE, the recombination of carriers) or the thermal generation of carriers in the dark is more harmful for the final application as the PLI is only able to capture recombination-active defects. Luckily, most generation centers are also recombination active.

While, here, we focused our analysis on completely processed Si photodiodes (photodetectors), the studies indicate that the exploitation of the PLI to various device fabrication steps as well as to other Si devices, where electrically active defects are harmful, is worth considering. Based on this study, the PLI can provide information that is not as easily available by other methods. In summary, these results indicate that PLI could find its use in the semiconductor industry for both fabrication process monitoring and final device characterization, which would save time, reduce costs, and increase high-quality production.

Acknowledgment

The authors acknowledge the provision of facilities by the Micronova Nanofabrication Centre, Espoo, Finland, within the OtaNano research infrastructure at Aalto University. The work is related to the Flagship on Photonics Research and Innovation "PREIN" funded by the Academy of Finland. A fruitful discussion with Thorsten Trupke and Robert Bardos is highly acknowledged. The assistance of Michael Serue and Daria Kriukova in conducting the EQE and I–V measurements is highly appreciated.

References

[1] H. Curtis and R. Verkuil, "A high signal-to-noise oscillator for contactless measurement of photoinduced carrier lifetimes," in *Proc. ASTM Int. Lifetime Factors silicon*, West Conshohocken, PA, USA, 1980, pp. 210–224.

[2] E. O. Johnson, "Measurement of minority carrier lifetimes with the surface photovoltage," *J. Appl. Phys.*, vol. 28, no. 11, pp. 1349–1353, Nov. 1957, doi: 10.1063/1.1722650.

[3] H. C. Gatos and J. Lagowski, "Surface photovoltage spectroscopy—A new approach to the study of high-gap semiconductor surfaces," *J. Vac. Sci. Technol.*, vol. 10, no. 1, pp. 130–135, Jan. 1973, doi: 10.1116/1.1317922.

[4] T. Trupke and R. A. Bardos, "Photoluminescence: A surprisingly sensitive lifetime technique," in *Proc. 21st IEEE Photovolt. Spec. Conf.*, Orlando, FL, USA, 2005, pp. 903–906.

[5] T. Trupke, R. A. Bardos, M. C. Schubert, and W. Warta, "Photoluminescence imaging of silicon wafers," *Appl. Phys. Lett.*, vol. 89, Jul. 2006, Art. no. 044107, doi: 10.1063/1.2234747.

[6] T. Trupke *et al.*, "Progress with luminescence imaging for the characterisation of silicon wafers and solar cells," in *Proc. 22nd Eur. Photovolt. Solar Energy Conf.*, Milan, Italy, 2007, pp. 22–31.

[7] T. Trupke and J. W. Weber, "Luminescence imaging: A powerful characterization tool for photovoltaic applications," in *Proc. SPIE*, vol. 7772, Aug. 2010, Art. no. 777202.

[8] T. Trupke, B. Mitchell, J. W. Weber, W. Mcmillan, R. A. Bardos, and R. Kroeze, "Photoluminescence imaging for photovoltaic applications," *Energy Proc.*, vol. 15, pp. 135–146, Sep. 2012, doi: 10.1016/j.egypro.2012.02.016.

[9] R. Duru *et al.*, "Photoluminescence imaging for buried defects detection in silicon: Assessment and use-cases," *IEEE Trans. Semicond. Manuf.*, vol. 32, no. 1, pp. 23–30, Feb. 2019, doi: 10.1109/TSM.2018.2871967.

[10] W. Shockley and W. T. Read, "Statistics of the recombination of holes and electrons," *Phys. Rev.*, vol. 87, pp. 835–842, Sep. 1952, doi: 10.1103/PhysRev.87.835.

[11] R. N. Hall, "Electron-hole recombination in germanium," *Phys. Rev.*, vol. 87, no. 2, p. 387, 1952, doi: 10.1103/PhysRev.87.387.

[12] P. V. Auger, "Sur les rayons β secondaires produits dans un gaz par des rayons X," *CR Acad. Sci.*, vol. 177, p. 169, Oct. 1923.

[13] J. Dziewior and W. Schmid, "Auger coefficients for highly doped and highly excited silicon," *Appl. Phys. Lett.*, vol. 31, no. 5, pp. 346–348, Sep. 1977, doi: 10.1063/1.89694.

[14] D. J. Fitzgerald and A. S. Grove, "Surface Recombination in semiconductors," *Surf. Sci.*, vol. 9, no. 2, pp. 347–369, 1968, doi: 10.1016/0039-6028(68)90182-9.

[15] Y. P. Varshni, "Band-to-band radiative recombination in groups IV, VI, and III-V semiconductors (I)," *Phys. Status Solidi B*, vol. 19, no. 2, pp. 459–514, 1967, doi: 10.1002/pssb.19670190202.

[16] D. K. Schroder, "Carrier lifetimes in silicon," *IEEE Trans. Electron Devices*, vol. 44, no. 1, pp. 160–170, Jan. 1997, doi: 10.1109/16.554806.

[17] R. Hall, "Recombination processes in semiconductors," *Proc. IEE-B, Electron. Commun. Eng.*, vol. 106, no. 17, pp. 923–931, Mar. 1959, doi: 10.1049/pi-b-2.1959.0171.

[18] P. P. Altermatt, F. Geelhaar, T. Trupke, X. Dai, A. Neisser, and E. Daub, "Injection dependence of spontaneous radiative recombination in crystalline silicon: Experimental verification and theoretical analysis," *Appl. Phys. Lett.*, vol. 88, no. 26, Jun. 2006, Art. no. 261901, doi: 10.1063/1.2218041.

[19] R. A. Bardos, T. Trupke, M. C. Schubert, and T. Roth, "Trapping artifacts in quasi-steady-state photoluminescence and photoconductance lifetime measurements on silicon wafers," *Appl. Phys. Lett.*, vol. 88, Feb. 2006, Art. no. 053504, doi: 10.1063/1.2165274.

[20] T. Roth, P. Rosenits, M. Rudiger, W. Warta, and S. W. Glunz, "Comparison of photoconductance and photo-luminescence-based lifetime measurement techniques," in *Proc. Conf. Optoelectron. Microelectron. Mater. Devices*, Sydney, NSW, Australia, 2008, pp. 249–252, doi: 10.1109/COMMAD.2008.4802138.

[21] P. J. Cousins, D. H. Neuhaus, and J. E. Cotter, "Experimental verification of the effect of depletion-region modulation on photoconductance lifetime measurements," *J. Appl. Phys.*, vol. 95, no. 4, pp. 1854–1858, Feb. 2004, doi: 10.1063/1.1638618.

[22] T. Trupke *et al.*, "Effective excess carrier lifetimes exceeding 100 ms in float zone silicon determined from photoluminescence," in *Proc. 19th European Photovolt. Solar Energy Conf.*, Paris, France, 2004, pp. 758–761.

[23] R. A. Sinton, A. Cuevas, and M. Stuckings, "Quasi-steady-state photoconductance, a new method for solar cell material and device characterization," in *Proc. 5th IEEE Photovolt. Spec. Conf.*, Washington DC, USA, 1996, pp. 457–460.

[24] R. A. Sinton and A. Cuevas, "Contactless determination of current–voltage characteristics and minority-carrier lifetimes in semiconductors from quasi-steady-state photoconductance data," *Appl. Phys. Lett.*, vol. 69, no. 17, pp. 2510–2512, Oct. 1996, doi: 10.1063/1.117723.

[25] S. Herlufsen, J. Schmidt, D. Hinken, K. Bothe, and R. Brendel, "Photoconductance-calibrated photoluminescence lifetime imaging of crystalline silicon," *Phys. Status Solidi*, vol. 2, no. 6, pp. 245–247, Dec. 2008, doi: 10.1002/pssr.200802192.

[26] J. A. Giesecke, M. C. Schubert, B. Michl, F. Schindler, and W. Warta, "Minority carrier lifetime imaging of silicon wafers calibrated by quasi-steady-state photoluminescence," *Sol. Energy Mater. Sol. Cells*, vol. 95, no. 3, pp. 1011–1018, Mar. 2011, doi: 10.1016/j.solmat.2010.12.016.

[27] D. K. Schroder, "The concept of generation and recombination lifetimes in semiconductors," *IEEE Trans. Electron Devices*, vol. ED-29, no. 8, pp. 1336–1338, Aug. 1982, doi: 10.1109/TED.1982.20879.

[28] T. Trupke, R. A. Bardos, M. D. Abbott, F. W. Chen, J. E. Cotter, and A. Lorenz, "Fast photoluminescence imaging of silicon wafers," in *Proc. IEEE 4th World Conf. Photovolt. Energy Conf.*, Waikoloa, HI, USA, Aug. 2006, pp. 928–931, doi: 10.1109/WCPEC.2006.279608.

[29] T. Trupke, R. Bardos, M. Abbott, F. Chen, K. Fisher, and J. Cotter, "Luminescence imaging: An ideal characterization tool for silicon," in *Proc. 16th Workshop Crystalline Silicon Sol. Cells Modules, Mater. Processes*, Denver, CO, USA, Aug. 2006, pp. 50–57.